JOURNAL OF GEOPHYSICAL RESEARCH, VOL. 90, NO. A7, PAGES 6409–6418, JULY 1, 1985

Test Particle Modeling of Wave-Induced Energetic Electron Precipitation

H. C. CHANG[1] AND U. S. INAN

Space, Telecommunications and Radioscience Laboratory, Stanford University, California

A test particle computer model of the precipitation of radiation belt electrons is extended to compute the dynamic energy spectrum of transient electron fluxes induced by short-duration VLF wave packets traveling along the geomagnetic field lines. The model is adapted to estimate the count rate and associated spectrum of precipitated electrons that would be observed by satellite-based particle detectors with given geometric factor and orientation with respect to the magnetic field. A constant-frequency wave pulse and a lightning-induced whistler wave packet are used as examples of the stimulating wave signals. The effects of asymmetry of particle mirror heights in the two hemispheres and the atmospheric backscatter of loss cone particles on the computed precipitated fluxes are discussed.

1. INTRODUCTION

A test particle computer model has recently been developed for quantitative evaluation of the flux level and the temporal signatures of wave-induced precipitation of radiation belt electrons [*Inan et al.*, 1982; *Chang et al.*, 1983]. This model has been applied for various magnetospheric and wave parameters and has been used to interpret observed correlations between waves and precipitation effects in the ionosphere [*Chang and Inan*, 1983*b*].

One to one correlations between electron precipitation or its ionospheric effects (X rays, photoemissions, density enhancements) and natural waves (whistlers, emissions) as well as man-made signals from VLF transmitters have been observed during ground- and satellite-based experiments [e.g., *Rosenberg et al.*, 1971; *Helliwell et al.*, 1973, 1980; *Rycroft*, 1973; *Imhof et al.*, 1983*a*, *b*; *Voss et al.*, 1984]. The observed correlations have been attributed to wave-induced precipitation resulting from cyclotron resonance wave-particle interactions in the magnetosphere.

The modeling results have previously been presented in terms of time evolution of precipitated electron energy fluxes incident on the ionosphere and integrated over a range of energies [*Chang and Inan*, 1983*b*]. This information is useful for estimating and interpreting integral effects on the ionosphere such as precipitation-induced light emissions measured by photometers [*Chang and Inan*, 1983*b*]. While energy flux levels can be inferred from the intensity of photometric emissions, measurements using balloon X ray detectors can be used to estimate the spectral characteristics of the precipitated flux [*Wei et al.*, 1984]. Crude spectral information can also be extracted from measurements of light emissions at multiple wavelengths [*Rees and Luckey*, 1974]. Theoretical estimation of precipitated flux spectra is needed for comparison with such data for the purpose of improving our understanding of the wave-induced scattering mechanism and for potential use as a diagnostic tool to study the energetic electron distribution in the magnetosphere. The spectral content of precipitation flux is also important in determining the ionospheric height at which the maximum perturbations should occur [*Banks et al.*, 1974].

On board low-altitude satellites or rockets, multichannel particle detectors can obtain detailed spectral information about precipitating electrons. The output of particle detectors is in terms of count rate as determined by the geometric factor and orientation of the particular detector. It is then of interest to estimate the count rate and spectrum of wave-induced precipitation that would be observed using a given detector.

In this paper we extend the test particle model to determine the dynamic spectrum of the transient electron energy flux precipitated in the ionosphere by short-duration VLF wave packets traveling along the geomagnetic field lines. We also consider a particle detector used in the Stimulated Energetic Electron Precipitation (SEEP) satellite program [*Imhof et al.*, 1983*a*] to compute the time development and spectral characteristics of the count rate of precipitated electrons that would be observed by this detector.

In most cases considered, we assume a geomagnetic field with mirror symmetry with respect to the equatorial plane and neglect the possible backscattering of particles as they interact with atmospheric constituents. We then separately discuss the effects of the asymmetry of the loss cones in the two hemispheres and atmospheric backscatter for one specific case.

2. CALCULATION OF WAVE-INDUCED PRECIPITATED ENERGY FLUX

Cyclotron Resonance Wave-Particle Interactions

We consider wave-induced perturbations of a distribution of energetic electrons trapped in the earth's magnetic field. The perturbations of the particle distribution near the loss

[1]Now at Department of Electrical Engineering, National Taiwan University, Taipei, Republic of China.

Paper number 4A8410.
0148-0227/85/004A-8410$05.00

cone are estimated by computing the pitch angle scattering of individual, near-resonant test particles.

Consider the case of a longitudinally propagating wave, that is, $\mathbf{k} \| \mathbf{B_0}$, where $\mathbf{k}$ is the wave vector and $\mathbf{B_0}$ is the static magnetic field. For longitudinal propagation, the cyclotron resonance condition is given by

$$f_H/\gamma \simeq f - \mathbf{k} \cdot \mathbf{v} \tag{1}$$

where f_H is the local electron gyrofrequency, $\mathbf{v}$ is the total velocity of the electron, $\gamma = (1 - v^2/c^2)^{-1/2}$ is the relativistic factor, and f is the wave frequency. For the whistler mode ($f < f_H$) wave and for the parameters of interest in this paper, (1) is satisfied when the electrons and the wave travel in opposite directions [*Chang and Inan*, 1983*a*].

Particle Distribution Function

We represent the energetic electron population in a magnetic flux tube by a distribution function $f(E, \alpha)$ defined at the equator, where E is the energy and α is the equatorial pitch angle of the particle. Using the first adiabatic invariant, the pitch angle and the velocity components of trapped particles can be determined at each point along the field line in terms of these equatorial values.

In many experiments the particle data are given in terms of the differential energy spectral intensity $\Phi(E, \alpha)$ in el $\mathrm{cm}^{-2}\ \mathrm{s}^{-1}\ \mathrm{sr}^{-1}\ \mathrm{keV}^{-1}$. We assume here that $\Phi(E, \alpha) = \Phi_E g(\alpha)$, i.e., Φ is separable in E and α, where $\Phi_E = \Phi(E, 90°)$ is a function of E and $g(\alpha)$ accounts for the anisotropy of Φ. It should be noted here that the assumption of a separable distribution is merely for convenience in the analytical representation and is not critical to the model calculations. This is especially true since only particles in a very narrow range above the loss cone contribute to the wave-induced precipitation. It can be shown [*Chang*, 1983] that

$$f(E, \alpha) = \Phi_E \frac{m {\gamma_E}^3}{v^2} g(\alpha) \tag{2}$$

where m is the rest mass of electron, γ_E is the relativistic factor associated with the energy E, or $\gamma_E = (E + mc^2)/mc^2$, and v is the magnitude of the velocity of an electron with energy E. Equation (2) indicates that for energies for which ${\gamma_E}^3 \simeq 1$, if Φ_E varies as v^{-n}, the distribution function is proportional to v^{-n-2}. Since $v^2/c^2 = ({\gamma_E}^2 - 1)/{\gamma_E}^2$, (2) can also be written as

$$f(E, \alpha) = \Phi_E \left(\frac{m}{c^2}\right) \left(\frac{{\gamma_E}^5}{{\gamma_E}^2 - 1}\right) g(\alpha)$$

The distribution function can be assumed to be described by a power law [e.g., *Chang and Inan*, 1983*a*]

$$f(E, \alpha) = \Phi_{E_0} \left(\frac{m}{c^2}\right) \left(\frac{{\gamma_{E_0}}^5}{{\gamma_{E_0}}^2 - 1}\right) {E_0}^{n/2} E^{-n/2} g(\alpha) \tag{3}$$

where E_0(in keV) is a given energy and $n/2$ is an exponent that determines the energy dependence of the distribution.

Alternatively, an exponential law for the differential energy spectral intensity may be assumed to fit the observed particle data. For this case, the spectral intensity is written as

$$\Phi_E = \Phi_0 e^{-E/E_0} \tag{4}$$

where Φ_0 is the spectral intensity at zero energy and E_0 is the characteristic energy or the e-folding energy.

In this paper we consider an initially empty loss cone so that $g(\alpha) = 0$ and therefore $f(E, \alpha) = 0$ for $\alpha < \alpha^{\mathrm{lc}}$ whereas $g(\alpha) = 1$ for $\alpha > \alpha^{\mathrm{lc}}$, where α^{lc} is the angular half width of the loss cone.

Test Particle Calculation of Transient Precipitation

We employ a test particle model [*Inan et al.*, 1978, 1982; *Chang et al.*, 1983] in which a large number of test particles distributed in $v_\parallel, \alpha$, and ϕ are used to represent a full distribution of electrons, where $v_\parallel$ is the equatorial velocity of particles parallel to the field line and the Larmor phase angle ϕ is defined as the angle between the particle perpendicular velocity $v\perp$ and the wave magnetic field $\mathbf{B}_\omega$. The trajectories of individual test particles under the influence of a wave are computed by numerically solving a set of equations of motion. The resulting perturbations of the particle distribution function are inferred from the scattering coefficients of individual test particles. This approach was used in the past to determine the time evolution of the precipitated energy fluxes (ergs $\mathrm{cm}^{-2}\ \mathrm{s}^{-1}$) induced by short-duration whistler mode wave pulses propagating along the earth's magnetic field lines [*Inan et al.*, 1982]. Here we extend this technique to determine the spectral content of the wave-induced precipitated energy flux.

The spectral intensity q_E (ergs $\mathrm{cm}^{-2}\ \mathrm{s}^{-1}\ \mathrm{keV}^{-1}$) of the precipitated energy flux that flows parallel to the field line into the ionosphere is obtained by integrating the quantity $Ev \cos \alpha_i f(E, \alpha)$ over the loss cone in velocity space [*Chang*, 1983],

$$q_E = \frac{2\pi}{\Delta E} \int_0^{\alpha^{\mathrm{lc}}} \int_{v_{\parallel -}}^{v_{\parallel +}} Ev \cos \alpha_i f(E, \alpha) \left[\frac{\cos \alpha}{\cos \alpha_i} \frac{B_i}{B\mathrm{eq}}\right] \cdot {v_\parallel}^2 \frac{\sin \alpha}{\cos^3 \alpha} dv_\parallel d\alpha \tag{5}$$

where $v_{\parallel +}$ and $v_{\parallel -}$ are respectively the parallel velocities corresponding to energies $E + \Delta E/2$ and $E - \Delta E/2$, so that

$$E \pm \Delta E/2 = mc^2[(1 - {v_{\parallel \pm}}^2/c^2 \cos^2 \alpha)^{-1/2} - 1]$$

B_i and α_i are the magnetic field strength and the pitch angle, respectively, at the ionospheric height, $B\mathrm{eq}$ is the mag-

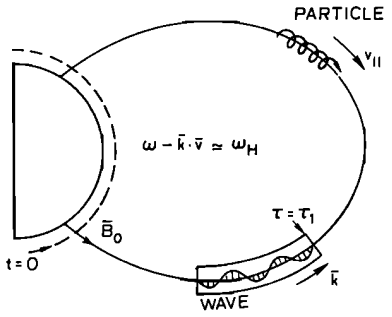

Fig. 1. Schematics showing the propagation of a VLF wave pulse and the travel of an energetic electron along a geomagnetic field line. The wave pulse is injected into the magnetosphere at time $t = 0$.

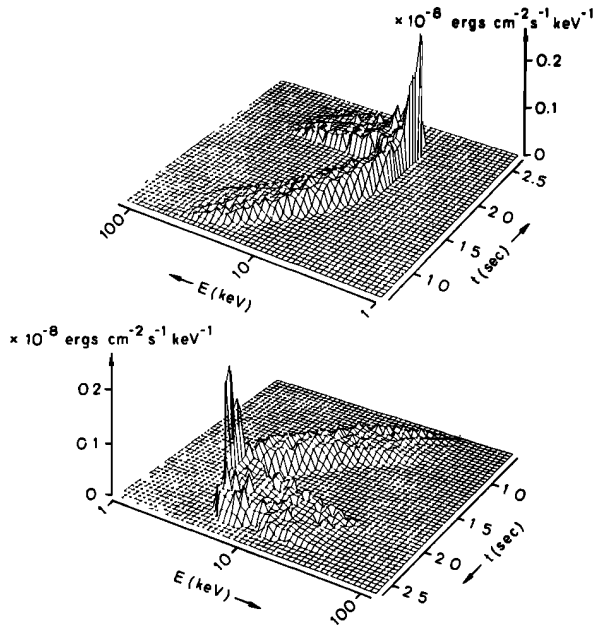

Fig. 2. Dynamic spectra of wave-induced flux, from two different perspectives, representing the evolution of energy flux as a function of energy and time for the case of a 0.5–s wave pulse propagating along the L=4 field line. These results were obtained by taking Φ_{E_0} = 1 el cm^{-2} s^{-1} sr^{-1} keV^{-1} for E=1 keV and E_0=10 keV in equation (4).

netic field strength at the equator; and ΔE is the desired energy resolution; in a realistic case this would be determined by the resolution of the experimental technique used in measuring such fluxes. Note that we have assumed a uniform distribution in ϕ and the 2π in (5) results from the integration over ϕ. The variables α and α_i are related by the adiabatic mirror equation $\sin^2 \alpha/B_{eq} = \sin^2 \alpha_i/B_i$. The factor $[(\cos\alpha/\cos\alpha_i)(B_i/B_{eq})]$ in (5), which can be obtained from the above mirror equation, accounts for the reduced volume element of the flux tube at the ionosphere compared to that at the equator. Note that q_E as defined in (5) represents the spectra to be observed near the wave injection site.

Time Evolution of Electron Energy Spectra

As an example, we consider a VLF wave pulse of 0.5-s duration which enters the magnetosphere at 1000 km altitude at time t = 0 and propagates along the L=4 field line, as depicted in Figure 1. An equatorial electron density of 400 el cm^{-3} and a diffusive equilibrium model for the cold plasma distribution [*Angerami and Carpenter*, 1966] are assumed. The earth's magnetic field is described by a centered dipole model. The wave frequency and the magnetic field intensity at the equatorial plane are taken to be 2.5 kHz and 5 pT respectively.

We present the result in terms of q_E as a function of energy E and time t. The initial trapped particle distribution is assumed to be of the exponential form with $\Phi_E = 10^0$ el cm^{-2} s^{-1} sr^{-1} keV^{-1} for E=1 keV and E_0=10 keV in (4). Particles are considered to be precipitated if their equatorial pitch angle after interacting with the wave is smaller than α_{lc}. In this particular case, particles for which $\Delta\alpha < 0.05°$ are assumed to be unaffected by the wave. This corresponds to a maximum electron energy of 60 keV, since particles having energies above 60 keV suffer pitch angle scatterings $\Delta\alpha < 0.05°$ and are thus assumed to be unperturbed by the wave.

As the input wave pulse propagates along the field line toward the equator, it first interacts with electrons of higher energies. This is because the resonant electron energy decreases as the wave approaches the equator in accordance with the resonance condition (1). These higher-energy electrons arrive at the precipitation region near the wave injection site earlier than those electrons scattered in the vicinity of the equator. The resulting energy precipitation in the form of q_E as a function of E and t after t = 0 is shown in Figure 2. The early arrival of higher-energy electrons is apparent. The two panels of Figure 2 give views of the same three-dimensional figure from two perspectives.

As the wave packet travels past the equator, it again interacts with higher-energy electrons and the resonant energy increases due to the variation of f_H with latitude. These higher-energy electrons, although interacting with the wave at later times, can overtake those electrons that have been scattered by the wave earlier near the equator. This "focusing" effect is evident in Figure 2 where electrons over a wide range of energies are shown to arrive at the precipitation region within a short time period after t = 2 s.

The top panel of Figure 3 shows the time evolution of the total precipitated energy flux in ergs cm^{-2} s^{-1} obtained by integrating q_E in Figure 2 over electron energy. As a result of the combined effects of the travel time of the wave and

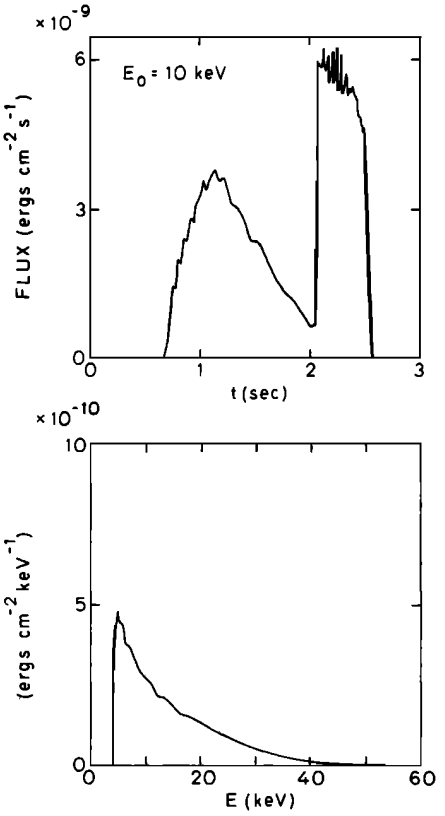

Fig. 3. Top panel shows the transient evolution of the precipitated energy flux as a function of time, obtained by integrating the dynamic spectrum in Figure 2 over the electron energy E. Bottom panel shows the spectrum of the precipitating electrons, obtained by integrating the same dynamic spectrum over time.

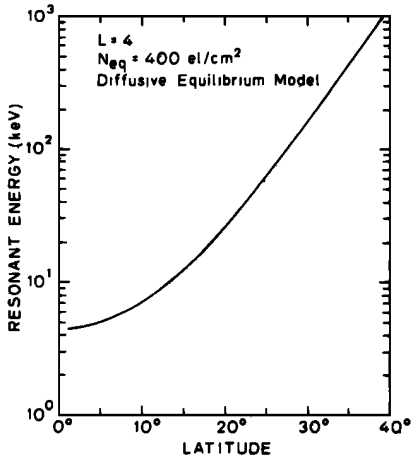

Fig. 4. Resonant energy as a function of latitude along the L=4 field line for a wave frequency of 2.5 kHz. An equatorial electron density of 400 el cm^{-3} and a diffusive equilibrium model for the cold plasma distribution are assumed.

the particles, the precipitation pulse appears to have a total duration of about 2 s, whereas the input wave pulse is only 0.5 s long. The focusing of the precipitating electrons discussed above results in a ~0.5-s long enhanced precipitated energy flux after $t = 2$ s.

The bottom panel of Figure 3 gives the spectrum of the precipitating electrons obtained by integrating q_E of Figure 2 over the time duration of the precipitation pulse. The result is presented in terms of ergs cm^{-2} keV^{-1} versus energy in keV and represents the time-integrated energy spectrum of the wave-induced precipitation pulse.

Resonant Energy Versus Latitude

The spectrum of the precipitating electrons shown in Figure 3 depends on the spectrum of Φ_E as well as the relative efficiency of the wave-induced scattering as a function of the location of the interaction region along the field as determined by the particle energy. The strong pitch angle scattering in the vicinity of the equatorial plane results in a sharp peak in the precipitated spectrum. Figure 4 shows the resonant electron energy as a function of latitude along the $L = 4$ field line for the case under study. For E=60 keV the wave-particle interaction region is located as far as 25° latitude off the equator, based on the assumption of a diffusive equilibrium model of the cold plasma distribution. However, the spectral magnitude (Figure 3) drops to half of the peak value at $E \simeq 12$ keV. Comparison of Figures 3 and 4 thus indicates that most of the downcoming electrons were scattered within approximately ±15° latitude. The sharp lower-energy cutoff in the spectrum of Figure 3 is due to the fact that particles having energies smaller than the equatorial resonant energy do not undergo a resonant interaction with this wave anywhere along the field line.

The transient flux shown in the top panel of Figure 3 can be considered to be composed of two separate parts, those arriving before and after $t \simeq 2$ s. They are due to wave-particle interactions on opposite sides of the equator, the one before $t \simeq 2$ s being on the downstream side of the particles. We have assumed that the total energy of the propagating wave packet is constant everywhere on the field line, i.e., that there is neither wave damping nor growth. It is known that monochromatic VLF waves can be amplified up to 30 dB near the geomagnetic equatorial plane as they traverse the interaction region [*Helliwell and Katsufrakis*, 1974]. If we postulate that the wave intensity is 20 dB lower than that used in the present calculation prior to the wave's traversal of the equator, the flux level of the first part in the top panel of Figure 3 would be reduced by an order of magnitude, since the precipitated energy flux tends to be proportional to the wave intensity [*Inan et al.*, 1982; *Chang et al.*, 1983].

Dependence on the e-Folding Energy

Up to now we have considered only the case of a trapped distribution with an e-folding energy $E_0 = 10$ keV in (4). To demonstrate the dependence on E_0, we present in Figure 5 energy flux versus time and the integrated spectrum for $E_0 = 50$ keV and $E_0 = 100$ keV. Other parameters for Figure 5 are the same as those of Figures 2 and 3. We have normalized Φ_E to $\Phi_E = 10^0$ el cm^{-2} s^{-1} sr^{-1} keV^{-1} at $E = 1$ keV so that the population of the trapped electrons above 1 keV will be larger for larger E_0 values.

The peak flux level for the $E_0 = 50$ keV case is found to be about 5 times higher than that of the $E_0 = 10$ keV case in Figure 3. Note that the flux scales in Figures 3 and 5 are different. For E_0=100 keV, the magnitude of the peak flux increases with no significant change in the pulse shape. The lower panels of Figure 5 clearly demonstrate the hardening of the precipitated spectra as the trapped spectrum is hardened, i.e., larger E_0.

3. WHISTLER-INDUCED PRECIPITATION

Our test particle simulation code is applicable to wave packets with slowly varying frequencies [*Chang et al.*, 1983*b*]. In the following we consider the case of a whistler wave pulse generated by a lightning discharge. The input impulsive

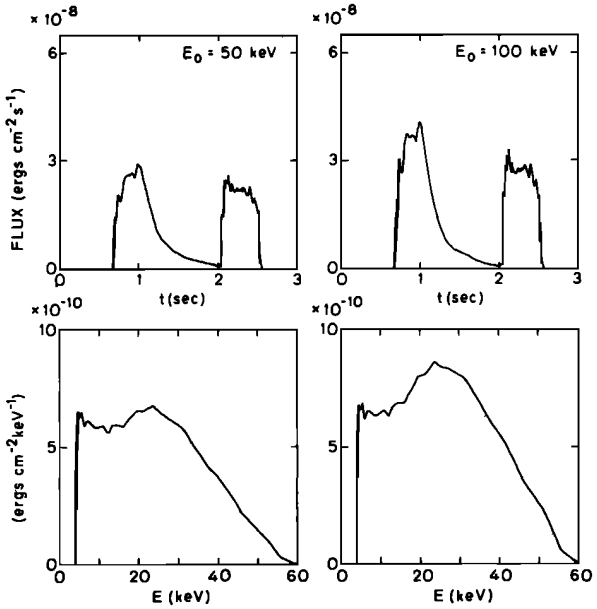

Fig. 5. Precipitated flux versus time and precipitated spectrum for E_0=50 and 100 keV. All other parameters have the same values as in Figure 3. The flux scale was chosen to be different from that of Figure 3.

electromagnetic wave energy is assumed to enter the magnetosphere at 1000-km altitude in the northern hemisphere at time t=0.

In this case the "duct" in which the whistler propagates is taken to lie along the L=3 field line. The wave energy propagates southward and arrives at the southern conjugate point as a one-hop whistler. The frequency range of the whistler is taken to extend from 500 Hz to 8.1 kHz, the latter being equal to one quarter of the equatorial gyrofrequency $f_{H\mathrm{eq}}$. Figure 6 shows the $f-t$ curve for this one-hop whistler that would be observed at the southern conjugate point after the injection of the impulse at t=0 in the north. Here we have used a diffusive equilibrium model and an equatorial electron density of 680 el cm^{-3} for the cold plasma distribution along the L=3 field line.

The power spectral density of the input wave impulse is assumed to be constant with frequency. In a separate study [*Chang and Inan*, 1985], whistler-induced precipitation over a wide range of L shells (L=2 to 4.5) was investigated. There, a more realistic distribution of the input wave power spectral density as a function of frequency was assumed. In this paper, however, we emphasize various aspects of the test particle simulation model rather than the geophysical implications of whistler-induced precipitation.

In the test particle model the total propagating energy of the wave packet in the duct is assumed to be conserved. The magnetic and electric field intensities of any wave frequency component at a given point along the field line depend on the local refractive index as well as the dispersion of the wave packet [*Chang et al.*, 1983]. For the present case, the absolute value of the product of the input wave power spectral density and the temporal duration of the impulse is taken to be 10^{-12} W m^{-2} Hz^{-1} s (or 10^{-12} joules m^{-2} Hz^{-1}), resulting in an equatorial wave magnetic field intensity $B_{W\mathrm{eq}}$ of ~15 pT at f=8.1 kHz.

Results in the same format as those shown in Figure 2 are given in Figure 7 for the whistler case. We use a power law with n=6 in (3) for the initial trapped particle distribution function. In order to estimate the order of magnitude of the absolute flux level, we consider a typical quiet time value for Φ_{E_0} of $\Phi_{E_0} \simeq 10^5$ el cm^{-2} s^{-1} sr^{-1} keV^{-1} at 90° pitch angle and $g(90°)/g(\alpha^{\mathrm{lc}}) \simeq 10$ for E_0=40 keV at $L \simeq 3$ [*Lyons and Williams*, 1975]. In this case we only consider electrons with energy less than 300 keV.

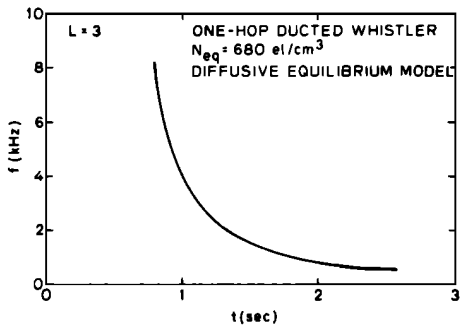

Fig. 6. The frequency-time curve of a one-hop whistler propagating along the L=3 field line with frequencies ranging from 500 Hz to 8.1 kHz, that would be observed at the southern conjugate point after the injection of a lightning impulse at t=0 in the north. A diffusive equilibrium model and an equatorial electron density of 680 el cm^{-3} were used.

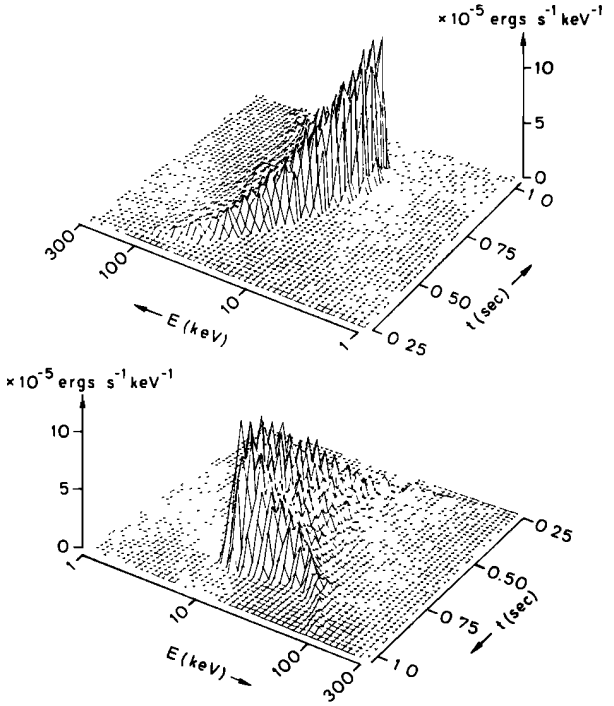

Fig. 7. Dynamic spectra of precipitated flux induced by the whistler wave described in Figure 6. A power law distribution with n=6 in equation (3) for the initial trapped distribution function is used. A typical quiet time value for Φ_{E_0} of $\Phi_{E_0} \simeq 10^5$ el cm^{-2} s^{-1} sr^{-1} keV^{-1} at 90° pitch angle and $g(90°)/g(\alpha^{\mathrm{lc}}) \simeq 10$ for E_0 = 40 keV at $L \simeq 3$ is assumed.

Figure 8*a* shows the precipitated energy flux versus time that would be observed near the wave injection site in the northern hemisphere. The peak flux is on the order of 10^{-3} ergs cm^{-2} s^{-1}. The spectrum of the precipitated flux obtained by integrating the dynamic spectrum in Figure 7 over time is shown in Figure 8*b*.

Precipitation in the Conjugate Hemisphere

We have so far considered the fluxes that would be precipitated near the wave injection site, i.e., the northern hemisphere in the present case. Particles scattered by south going waves could also be precipitated in the southern hemisphere due to their backscattering from the atmosphere in the north and/or their mirroring in the north due to the asymmetry in the earth's magnetic field strength.

For the whistler case we show in Figure 8*c* the mirrored precipitation flux that would be observed at the conjugate point in the south assuming that all the scattered electrons considered in Figure 8*a* mirror in the north and precipitate in the south. The mirrored precipitation pulse has a longer duration than that for the direct precipitation (Figure 8*a*) as a result of the dispersion of electrons having different energies. The time-integrated spectrum of the precipitated flux for the mirrored case is identical to that shown in Figure 8*b*, since the same precipitated electrons are involved in both cases.

Precipitation Over Different Energy Ranges

The energy fluxes calculated up to now consist of all precipitated electrons with energies below 300 keV. In Figure

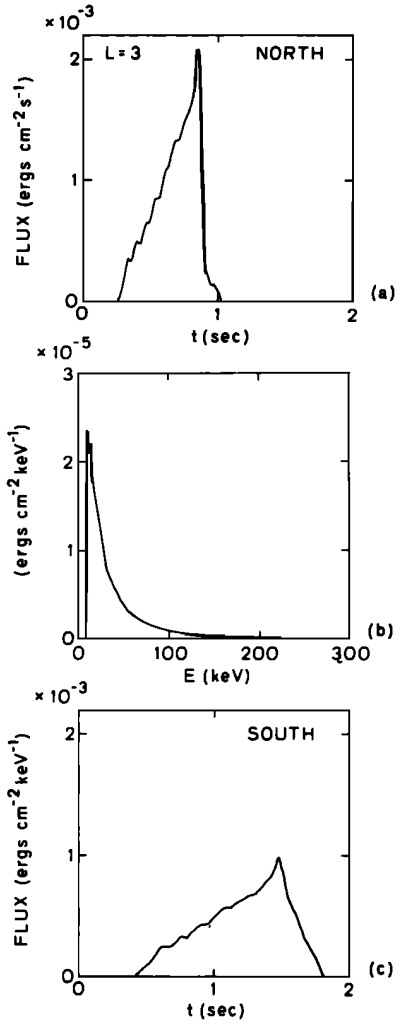

Fig. 8. (*a*) The transient precipitated flux in the north induced by the whistler wave, obtained by integrating the dynamic spectrum of Figure 7 over E. (*b*) The spectrum of the precipitating electrons, obtained by integrating the same dynamic spectrum over time. (c) The transient flux in the south if all the precipitated electrons are deposited in the south.

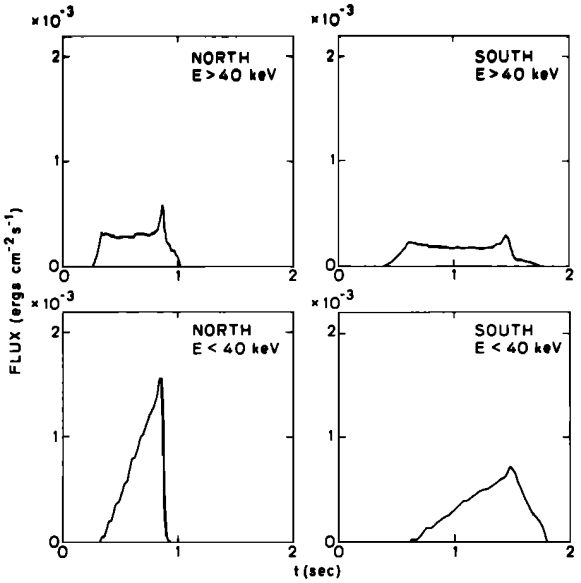

Fig. 9. Precipitated fluxes contributed by electrons with $E > 40$ keV and $E < 40$ keV for the whistler case. Left panels are for precipitation in the north.

9 we show the fluxes contributed by electrons with $E < 40$ keV and $E > 40$ keV, respectively, again for the whistler case. The left-hand panels represent precipitation near the wave injection site and correspond to the case of Figure 8*a*; those on the right represent precipitation near the conjugate point and correspond to that of Figure 8*c*. The transient fluxes for $E < 40$ keV show gradual buildup while that for $E > 40$ keV is relatively constant in time. Electrons with energies greater than 40 keV are able to penetrate deep into the ionosphere and perturb the ionospheric D region (80–90 km height) [*Banks et al.*, 1974]. One of the resulting effects is perturbation of subionospheric VLF/LF signal propagation, due to the enhanced ionization at the D region heights of wave reflection [*Helliwell et al.*, 1973].

The Effect of Mirror Height Asymmetry

In the above discussion of precipitation in the conjugate hemisphere, we have assumed that all electrons in the loss cone mirror and/or backscatter in the north and precipitate in the south. Under realistic conditions a part of these electrons would be precipitated in the north and a part would travel back to the south, depending on local atmospheric backscatter and mirror altitudes. The role of backscatter will be discussed in the next subsection; here we consider only the effect of mirror height asymmetry.

At geographic longitudes near the South Atlantic magnetic anomaly the mirror heights of particles in the north are known to be higher than those in the south due to an asymmetry in the earth's magnetic field strength [*Barish and Wiley*, 1970]. The difference between the southern and northern equatorial loss cone angles $\Delta\alpha^{lc} = \alpha_S^{lc} - \alpha_N^{lc}$ is a measure of the amount of asymmetry of the conjugate magnetic field strength. If a particle traveling northward does not undergo an equatorial pitch angle scattering greater than $\Delta\alpha^{lc}$, it would not precipitate in the north.

Figure 10 shows the peak value flux F_P of the transient precipitated energy flux and the integrated energy deposi-

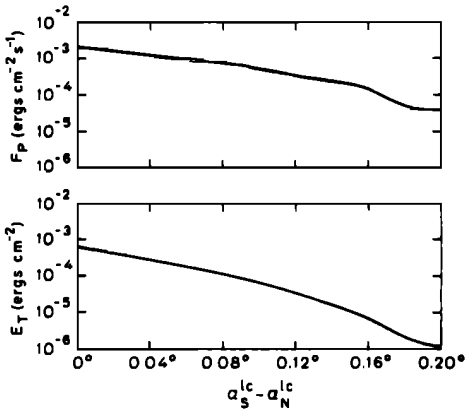

Fig. 10. Peak flux F_P to be observed in the northern hemisphere and integrated energy deposition E_T of the transient flux for the whistler case as functions of the difference between the southern and northern equatorial loss cone angles $\alpha_S^{lc} - \alpha_N^{lc}$.

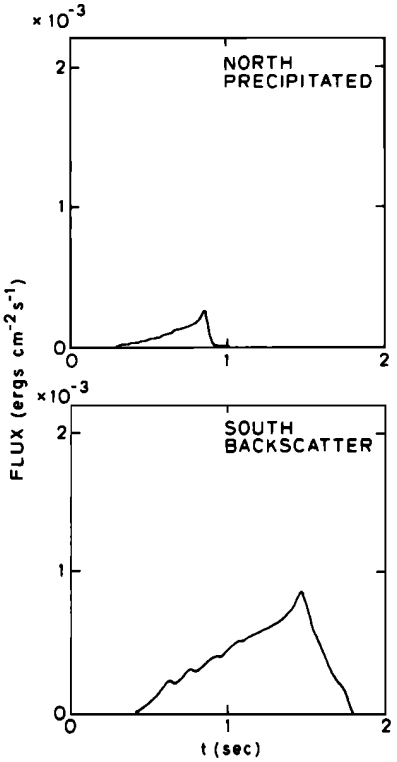

Fig. 11. Top panel shows the flux precipitated in the north for the whistler case when the atmospheric backscatter is taken into account. Bottom panel shows that part of the flux that backscatters in the north and enters the southern atmosphere.

tion E_T (in ergs cm^{-2}) (obtained by integrating the transient flux over time), as functions of $\Delta\alpha^{lc}$ for the whistler case. Here we only consider precipitation in the northern hemisphere. The result for $\Delta\alpha^{lc} = 0°$ corresponds to that shown in Figure 8*a*. As the mirror height difference $\Delta\alpha^{lc}$ increases, both F_P and E_T decrease, since more particles mirror back. The decrease of E_T is more pronounced because both the peak flux and the duration of the precipitation pulse are reduced.

It should be noted that the variations of F_P and E_T with respect to the mirror height difference depend significantly on the wave intensity within the wave-particle interaction region. For larger wave intensities more electrons should be able to overcome the mirror height difference, and consequently, F_P and E_T should decrease more gradually as functions of $\Delta\alpha^{lc}$.

This aspect of the problem and the role of the pitch angle distribution in the vicinity of the loss cone were discussed in a recent paper concerning comparison of model results with satellite data [*Inan et al.*, 1985].

The Effect of Atmospheric Backscatter

In the preceding sections we have assumed all particles with $\alpha_{eq} < \alpha_{eq}^{lc}$ to be precipitated into the atmosphere. However, theoretical calculations [e.g., *Stadsnes and Maehlum*, 1965; *Berger et al.*, 1974; *Davidson and Walt*, 1977] indicate that a fraction of particles within the loss cone can backscatter from the atmosphere. This should be particularly the case for wave-induced scattering of particles near the vicinity of the equatorial loss cone, since the fractional atmospheric backscatter can be as high as 80 – 90% for electrons that encounter the atmosphere at grazing pitch angles.

To incorporate this process in the estimation of transient precipitation fluxes, we assume the fractional population of particles backscattered to be given by $(1 - \cos\alpha)$, where α is the local particle pitch angle. This function closely approximates the pitch angle dependent fractional backscatter results obtained by *Berger et al.* [1974]. The top panel of Figure 11 shows the flux precipitated in the north for the case of Figure 8*a* when such backscatter is taken into account. It is seen that only a small fraction of electrons within the northern loss cone are precipitated, indicating that most of the scattered electrons are still near the edge of the loss cone. The bottom panel of Figure 11 shows the electron energy flux that backscatters in the north and arrives onto the southern hemisphere. If backscatter in the south is consid-

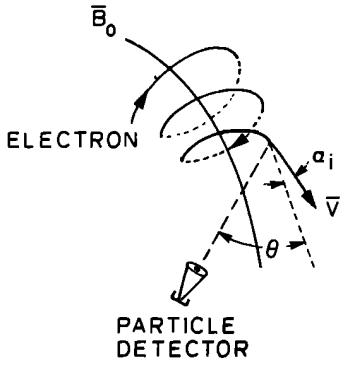

Fig. 12. Sketch showing the orientation of a particle detector and the motion of an electron near the precipitation region.

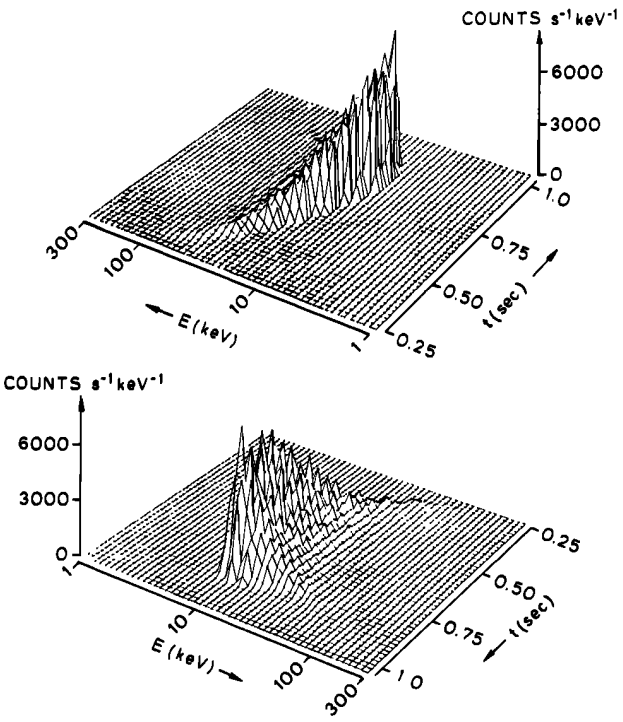

Fig. 13. Dynamic spectra of count rate as a function of E and t for the whistler case that would be recorded using the SEEP detector with $\theta = 90°$.

ered in a similar manner, only a small fraction of this south going flux would precipitate in the south. In making these estimates we have assumed that the backscattered particles undergo negligible energy or pitch angle change during the interaction with the atmosphere.

If we also include the effect of the mirror height asymmetry, the flux precipitated in the north would be even smaller than that shown in Figure 11, and the backscattered flux would increase slightly, depending on the degree of asymmetry as discussed in connection with Figure 10.

4. Modeling of Satellite-Based Experiments

The quantities considered above, namely the energy deposition rate in ergs cm^{-2} s^{-1} versus time and the spectrum in ergs cm^{-2} s^{-1} keV^{-1}, represent electron fluxes into the ionosphere parallel to the geomagnetic field lines and are useful for understanding the ionospheric effects of wave-induced precipitation as well as for studying these effects with ground- or balloon-based instruments.

Precipitating electrons can also be directly observed using particle detectors on board satellites or rockets. In the recent SEEP experiments, pulses of precipitation were found to be correlated with signals from a ground-based VLF transmitter [*Imhof et al.*, 1983*a*, *b*] and with lightning-generated whistlers [*Voss et al.*, 1984]. To better understand the relationship between the waves and the particles recorded by such detectors, it is important to use our theoretical model to estimate the electron count rates that should be measured in given detector configurations.

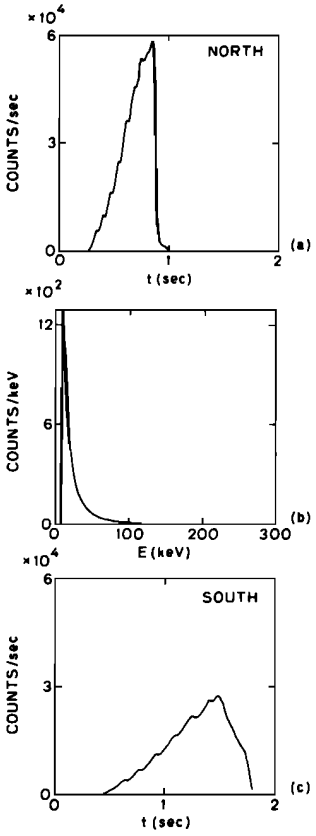

Fig. 14. (*a*) Count rate as a function of time for the whistler case, obtained by integrating the dynamic spectrum of Figure 13 over E. (*b*) The spectrum of the counts, obtained by integrating the same dynamic spectrum over time. (*c*) Count rate in the south if all the precipitated electrons are deposited in the south.

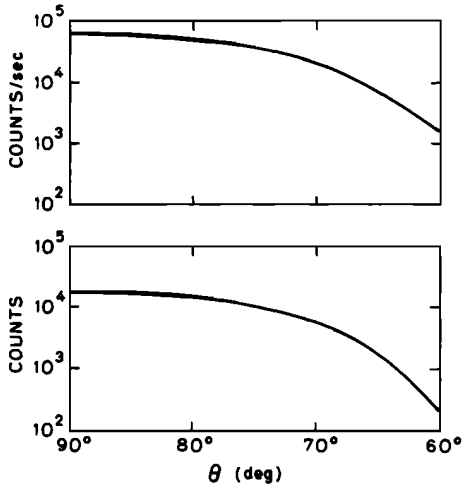

Fig. 15. Peak count rate and the time-integrated count rate (to be observed in the northern hemisphere) as a function of θ.

In the following, we calculate the count rate of precipitated electrons that would be detected by one of the particle detectors used in the SEEP satellite experiment [*Voss et al.*, 1982]. This detector has a geometric factor 0.17 cm^2 sr and an acceptance half angle of 20°. Figure 12 shows a sketch of the position of the detector relative to the field line at the satellite altitude. The angle between the direction of the field line and the axis of the detector is denoted by θ, and α_1 is the local pitch angle of downcoming electrons. An equation similar to (5) can be written for the dynamic spectrum of the count rate $C_E(\theta)$ (counts s^{-1} keV^{-1}) recorded by such a detector when its axis is in the θ direction:

$$C_E(\theta) = \frac{1}{\Delta E}\int_{\sigma()\neq o}\int_{v_{\|-}}^{v_{\|+}} vf(E,\alpha)\sigma(|\,\alpha_i - \theta\,|) \cdot \frac{1}{\sin\alpha_i}\left[\frac{\cos\alpha}{\cos\alpha_i}\frac{B_i}{B\text{eq}}\right] v_{\|}^2 \frac{\sin\alpha}{\cos^3\alpha} dv_{\|} d\alpha \tag{6}$$

where $\sigma()$, a function of the angle from the axis of the detector, is in units of cm^2 rad and represents the geometric factor integrated over the azimuthal angle and where other variables are as defined in connection with (5). The integrals of (6) are taken over the $v_{\|}$ range corresponding to a given energy range ΔE and over the equatorial pitch angle α for which $|\,\alpha_i - \theta\,| < 20°$, or $\sigma() \neq 0$.

Using the whistler case as an example, we consider the SEEP detector located near the precipitation region in the northern hemisphere with $\theta \simeq 90°$.

The dynamic spectra of the count rate as a function of E and t are shown in Figure 13, which is to be compared with Figure 7. Results similar to those of Figure 8 are shown in Figure 14, which is obtained by integrating the dynamic spectra of Figure 13 over time or energy.

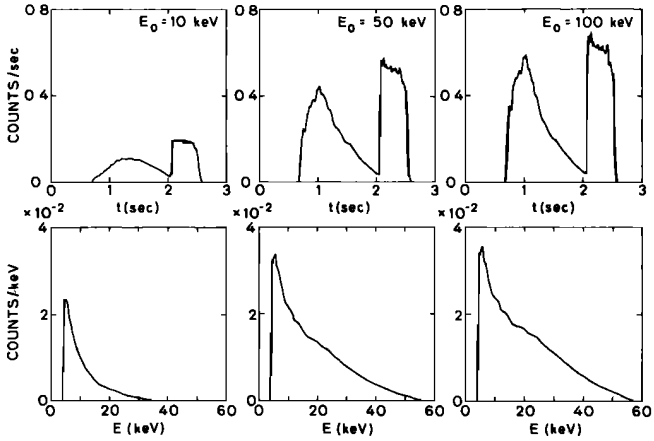

Fig. 16. The count rate versus time and the spectra of counts for the constant frequency cases shown in Figures 2 to 5. Three e-folding energies, i.e., E_0 = 10, 50, and 100 keV, are considered, and $\theta = 90°$ is assumed.

To show the variation of the count rate as a function of the orientation of the detector, we plot in Figure 15 the peak count rate and the time-integrated count rate recorded in the northern hemisphere, as a function of θ. These quantities are the counterparts of F_P and E_T shown in Figure 10. All wave, particle, and medium parameters are otherwise the same. The rapid drop of both quantities for $\theta > 70°$ indicates that in the present case the precipitated electrons are not scattered deeply into the loss cone, i.e., individual particle scatterings ($\Delta\alpha$) are relatively small. The same conclusion was reached in the discussion in connection with Figure 10. This result demonstrates that in attempting to detect wave-induced precipitation, detectors oriented at or close to 90° with respect to the magnetic field would be desirable.

For the sake of comparison, we present in Figure 16 the count rate versus time as well as the spectra of counts for the constant frequency cases discussed in Figures 2–5 again for the same detector. Three e-folding energies, i.e., E_0 = 10, 50, and 100 keV, are used, with all other parameters being identical to those used in the previous section. The detector orientation angle θ is taken to be 90°.

5. SUMMARY

We have reported the recently developed features of a test particle computer simulation model of gyroresonant wave-induced pitch angle scattering in the magnetosphere. This model has been used to predict the temporal evolution of precipitated electron energy fluxes induced by whistler mode wave packets propagating along geomagnetic field lines. New aspects of the model include the calculation of the dynamic energy spectra of precipitation, the modeling of count rates of precipitated electrons that would be observed using a specific particle detector on board a low-altitude satellite, and the inclusion of effects such as atmospheric backscatter and mirror height asymmetry.

The results presented in this paper demonstrate the versatility of the test particle model in terms of its application for interpreting observations using ground-, balloon-, satellite-, or rocket-based instruments. The predicted dynamic spectra of precipitation pulses often have characteristic shapes that in themselves can be useful in identifying such events. We hope that future experiments can be designed with the necessary high time and energy resolution so as to measure such detailed features. For low-altitude satellite- or rocket-based experiments our results clearly demonstrate the need for using detectors oriented near 90° with respect to the local direction of the magnetic field.

In terms of ground-based observations the test particle model can be used to study the characteristics of ionospheric effects of wave-induced particle precipitation, for example using riometer measurements or measurements of associated subionospheric signal perturbations (i.e., "Trimpi effects"). The time of onset of such perturbations with respect to the wave source can easily be estimated and compared with data. More importantly, the dynamic spectra of the precipitation bursts would determine the ionospheric altitude ranges that would be affected at different times. Thus, detailed comparison with data can be potentially useful in improving our ability to detect such events.

Through the comparison of model predictions with experimental data we can expect to improve our understanding of the gyroresonance wave-particle interaction mechanism. Ultimately, it may be possible to use the observed dynamic spectra of precipitation induced by waves for diagnostics of the trapped energetic particle distribution.

Acknowledgments. We acknowledge many discussions with our colleagues in the STAR Laboratory. This work was supported by the National Aeronautics and Space Administration under grant NGL-05-020-008. The work of one of us (H. C. Chang) was also partly supported by the Fleischmann Foundation. The typescript was prepared by N. Leger.

The Editor thanks J. C. Siren and another referee for their assistance in evaluating this paper.

REFERENCES

Angerami, J. J., and D. L. Carpenter, Whistler studies of the plasmapause in the magnetospheric ionization, *J. Geophys. Res., 71,* 711, 1966.

Banks, P. M., C. R. Chappell, and A. F. Nagy, A new model for the interaction of auroral electrons with the atmosphere: Spectral degradation, backscatter, optical emission, and ionization, *J. Geophys. Res., 79,* 1495, 1974.

Barish, F. D., and R. E. Wiley, World contours of conjugate mirror locations, *J. Geophys. Res., 75,* 6342, 1970.

Berger, M. J., S. M. Seltzer, and K. Maeda, Some new results on electron transport in the atmosphere, *J. Atmos. Terr. Phys., 36,* 591, 1974.

Chang, H. C., Cyclotron resonant scattering of energetic electrons by electromagnetic waves in the magnetosphere, *Tech. Rep. E414-1,* Space, Telecommun. and Radiosci. Lab., Stanford Univ., Stanford, Calif., 1983.

Chang, H. C., and U. S. Inan, Quasi-relativistic electron precipitation due to interactions with coherent VLF waves in the magnetosphere, *J. Geophys. Res., 88,* 318, 1983*a*.

Chang, H. C., and U. S. Inan, A theoretical model study of observed correlations between whistler mode waves and energetic electron precipitation events in the magnetosphere, *J. Geophys. Res., 88,* 10,053, 1983*b*.

Chang, H. C., and U. S. Inan, Lightning-induced electron precipitation from the magnetosphere, *J. Geophys. Res., 90,* 1531, 1985.

Chang, H. C., U. S. Inan, and T. F. Bell, Energetic electron precipitation due to gyroresonant interactions in the magnetosphere involving coherent VLF waves with slowly varying frequency, *J. Geophys. Res., 88,* 7037, 1983.

Davidson, G., and M. Walt, Loss cone distributions of radiation belt electrons, *J. Geophys. Res., 82,* 48, 1977.

Helliwell, R. A., and J. P. Katsufrakis, VLF wave injection into the magnetosphere from Siple Station, Antarctica, *J. Geophys. Res., 79,* 2511, 1974.

Helliwell, R. A., J. P. Katsufrakis, and M. L. Trimpi, Whistler-induced amplitude perturbation in VLF propagation, *J. Geophys. Res., 78,* 4679, 1973.

Helliwell, R. A., S. B. Mende, J. H. Doolittle, W. C. Armstrong, and D. L. Carpenter, Correlations between λ4278 optical emissions and VLF wave events observed at $L \sim 4$ in the Antarctic, *J. Geophys. Res., 85,* 3376, 1980.

Imhof, W. L., J. B. Reagan, H. D. Voss, E. E. Gaines, D. W. Datlowe, J. Mobilia, R. A. Helliwell, U. S. Inan, and J. P. Katsufrakis, Direct observation of radiation belt electrons precipitated by the controlled injection of VLF signals from a ground-based transmitter, *Geophys. Res. Lett., 10,* 361, 1983*a*.

Imhof, W. L., J. B. Reagan, H. D. Voss, E. E. Gaines, D. W. Datlowe, J. Mobilia, R. A. Helliwell, U. S. Inan, and J. P. Katsufrakis, The modulated precipitation of radiation belt electrons by controlled signals from VLF transmitters, *Geophys. Res. Lett., 10,* 615, 1983*b*.

Inan, U. S., T. F. Bell and R. A. Helliwell, Nonlinear pitch angle scattering of energetic electrons by coherent VLF waves in the magnetosphere, *J. Geophys. Res., 83*(A7), 3137, 1978.

Inan, U. S., T. F. Bell, and H. C. Chang, Particle precipitation induced by short-duration VLF waves in the magnetosphere, *J. Geophys. Res., 87,* 6243, 1982.

Inan, U. S., H. C. Chang, R. A. Helliwell, W. L. Imhof, J. B. Reagan, and M. Walt, Precipitation of radiation belt electrons by man-made waves: A comparison between theory and measurement, *J. Geophys. Res., 90,* (A1), 359, 1985.

Lyons, L. R., and D. J. Williams, The quiet time structure of energetic (35-560 keV) radiation belt electrons, *J. Geophys. Res., 80,* 943, 1975.

Rees, M. H., and D. Luckey, Auroral electron energy derived from rates of spectroscopic emissions, 1, Model computations, [*J. Geophys. Res., 79,* 5181, 1974.

Rosenberg, T. J., R. A. Helliwell, and J. P. Katsufrakis, Electron precipitation associated with discrete very-low-frequency emissions, *J. Geophys. Res., 76,* 8445, 1971.

Rycroft, M. J., Enhanced energetic electron intensities at 100 km altitude and a whistler propagating through the plasmapause, *Planet. Space Sci., 21,* 239, 1973.

Stadsnes, J., and B. Maehlum, Scattering and absorption of fast electrons in the upper atmosphere, internal report, Norw. Def. Res. Estab., Kjeller, Norway, 1965.

Voss, H. D., J. B. Reagan, W. L. Imhof, D. O. Murray, D. A. Simpson, D. P. Cauffman, and J. C. Bakke, Low temperature characteristics of solid state detectors for energetic X ray, ion and electron spectrometers, *IEEE Trans. Nucl. Sci., NS-29,* 164, 1982.

Voss, H. D., W. L. Imhof, J. Mobilia, E. E. Gaines, M. Walt, U. S. Inan, R. A. Helliwell, D. L. Carpenter, J. P. Katsufrakis, and H. C. Chang, Lightning-induced electron precipitation, *Nature, 312,* 740, 1984.

Wei, R., D. L. Detrick, T. J. Rosenberg, and U. S. Inan, Dynamic energy spectra of wave-induced electron precipitation, *Eos Trans. AGU, 65,* 1062, 1984.

H. C. Chang, Department of Electrical Engineering, National Taiwan University, Taipei, Taiwan, Republic of China.

U. S. Inan, Space, Telecommunications and Radioscience Laboratory, Stanford University, Stanford, CA 94305.

(Received November 9, 1984;
revised February 18, 1985;
accepted March 18, 1985.)